USING A SUITE OF OBSERVATIONAL AND FORECASTING TOOLS TO STUDY A SEA / LAND BREEZE EVENT

Jonathan L. Case*, Winifred C. Lambert,
NASA Kennedy Space Center / Applied Meteorology Unit / ENSCO, Inc.

John E. Lane, Christopher D. Immer,
ASRC Aerospace

Francis J. Merceret, and Jennifer G. Ward
NASA Kennedy Space Center

1. INTRODUCTION

Space launch, landing, and ground operations at the Kennedy Space Center (KSC) and Cape Canaveral Air Force Station (CCAFS) are highly sensitive to mesoscale weather conditions throughout the year. The complex topography and land-sea interfaces across KSC/CCAFS often lead to the development of mesoscale phenomena such as sea, river, and land breezes. These phenomena modify the prevailing synoptic wind, temperature, and stability fields, and can substantially impact space operations through sudden wind shifts and/or convective initiation. Due to the complex topography and the important role of mesoscale circulations during spacelift operations, a high-resolution network of 44 wind towers and five 915-MHz Doppler Radar Wind Profilers (DRWP) has been installed over the KSC/CCAFS area. This observational network helps forecasters to monitor the evolution of important mesoscale phenomena with precision. In addition, a local high-resolution configuration of the Regional Atmospheric Modeling System (RAMS; Pielke et al. 1992) numerical weather prediction (NWP) model provides daily forecast guidance on the development and evolution of these phenomena.

Recent efforts by the Applied Meteorology Unit (AMU) and personnel formerly of Dynacs, Inc. (currently with ASRC Aerospace) have studied various mesoscale phenomena across KSC/CCAFS utilizing the unique combination of available observational and modeling tools. To assess the statistical properties of boundary-layer wind changes, quality-control (QC) routines developed and modified by the AMU for the 915-MHz DRWPs were used to remove erroneous data prior to analysis. Examination of the quality-controlled data revealed the profiler network's ability to provide high temporal resolution observations of the vertical structure of several mesoscale phenomena including sea and land breezes, low-level jets, and frontal passages. In a recent AMU study, quality-controlled wind tower and 915-MHz DRWP data were used to examine the structural characteristics of nocturnal land breezes, and to develop a seven-year land-breeze composite that

Corresponding author address: Jonathan Case, ENSCO, Inc., 1980 N. Atlantic Ave., Suite 230, Cocoa Beach, FL 32931. Email: case.jonathan@ensco.com

provides climatological tools for predicting the land-breeze occurrence, timing, and movement. Finally, personnel from Dynacs Inc. and the AMU developed an objective technique to detect sea-breeze boundaries within the tower network, and to verify these boundaries as predicted by RAMS. The technique was designed to improve the objective verification of NWP models by creating an automated, phenomenological-based validation tool.

This paper presents an integrated analysis of a multi-day sea/land breeze event from 10−13 May 2000 using the unique combination of observational data and forecast verification tools described above. Section 2 describes the available observational and forecast data used for the analysis and explains the QC algorithms applied to the data. The technique used to verify the RAMS forecast sea-breeze transitions is presented in Section 3. Selected tower, profiler, and verification results from the multi-day event are presented in Section 4, and Section 5 provides a summary.

2. OBSERVATIONAL AND FORECAST DATASETS

This section describes a portion of the unique observational data network across KSC/CCAFS and the high-resolution RAMS forecast data that were verified by the tower observations for sea-breeze predictions.

2.1 Towers and 915-MHz profilers

The KSC/CCAFS wind tower network consists of 44 observational towers (Fig. 1). The towers in the network have an average station spacing of 5 km and contain sensors to measure temperature, dew point, and winds at various levels ranging from 1.8 m to 150 m. The primary measurement levels for most towers are 1.8 m (temperature and dew point), 3.6 m (winds), and 16.5 m (winds and temperature). The temporal resolution of the archived data is 5 minutes.

A network of five 915-MHz DRWPs with Radio Acoustic Sounding Systems was installed on KSC/CCAFS to provide wind estimates in the data gap between the top of the tower network at 150 m and the lowest gate of the NASA 50-MHz DRWP at ~2 km (Heckman 1996). The profilers are arranged in a diamond-like pattern over the KSC/CCAFS area with an average spacing of 10−15 km (Fig. 1). They provide

wind estimates using a consensus averaging technique from 130 m to as high as 6 km, depending on the configuration (Radian International 2001) and atmospheric conditions. The gate-to-gate resolution of the profilers is 100 m and the temporal resolution is 15 minutes.
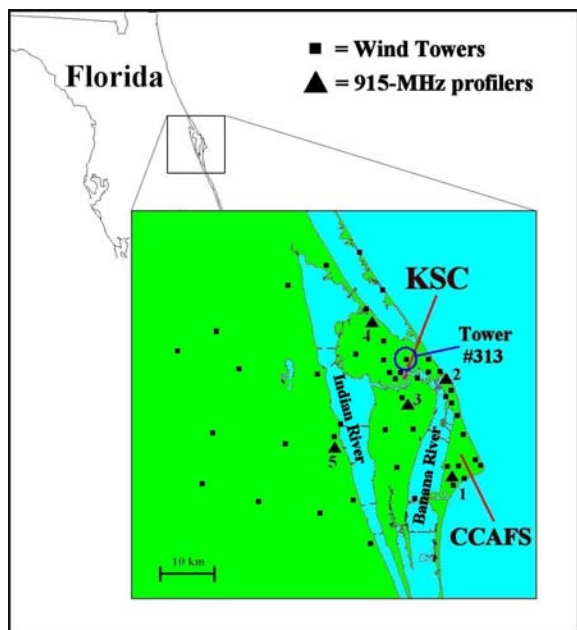
Figure 1. Locations of the 44 towers (squares) and five 915-MHz profilers (triangles) used to analyze the multi-day sea-land breeze event over east-central Florida. The locations of important geographical features and tower #313 are also indicated.

2.2 Quality-Control Algorithms

Erroneous observations were removed from the tower and 915-MHz profiler data sets prior to analysis. A different set of QC algorithms were used for each data set.

Five QC routines developed within the AMU specifically for the KSC/CCAFS tower network were used to QC the data (Lambert 2002): an unrealistic value check, a standard deviation check, a peak-to-average wind speed ratio check, a vertical consistency check, and a temporal consistency check.

The 915-MHz DRWP data were subjected to a set of automated QC algorithms (Lambert et al. 2003) based on the quality assessment routines described in Lambert and Taylor (1998), followed by a rigorous manual QC. The automated QC included checks of the length of the consensus averaging period, signal-to-noise ratio, unrealistic values, possible rain contamination, vertical shear magnitude, and spatial and temporal consistency.

2.3 RAMS Forecast Data

The three-dimensional, non-hydrostatic mode of RAMS (version 4a) was run on four nested grids with a horizontal grid spacing of 60, 15, 5, and 1.25 km (Fig. 2). RAMS uses a stretched vertical coordinate from near the surface up to 18 195 m, with additional vertical levels in grids 3 and 4 to provide enhanced vertical resolution near the ground. The physical parameterization schemes used in RAMS include a microphysics scheme (Cotton et al. 1982), a modified Kuo cumulus convection scheme (Tremback 1990), the Chen and Cotton (1988) radiation scheme, a Mellor and Yamada (1982) type turbulence closure, and an 11-layer soil-vegetation model (Tremback and Kessler 1985) with fixed soil moisture in the initial condition. The modified Kuo scheme is run on grids 1–3 whereas grid 4 utilizes explicit convection only. The mixed-phase microphysics scheme is run on all four grids.

In the operational setting, RAMS is initialized twice-daily at 0000 and 1200 UTC using the Eta 12-h forecast grids from its forecast cycle 12 hours earlier (due to operational time constraints), as well as available national and local observational data. Observational data are analyzed onto hybrid coordinates using the RAMS Isentropic Analysis (ISAN) package (Tremback 1990). The ISAN hybrid coordinate consists of a combination of isentropes and terrain-following surfaces on which data are analyzed within the RAMS model domain, similar to the NCEP Rapid Update Cycle model (Benjamin et al. 1998).

For sea-surface temperature initialization, RAMS uses fixed monthly climatological means on grid 1, and these values are subsequently interpolated to the inner grids. The lateral boundary conditions are nudged (Davies 1983) by 12–36-h forecasts from the NCEP Eta model, interpolated onto an 80-km grid, using two-way interactive boundary conditions.
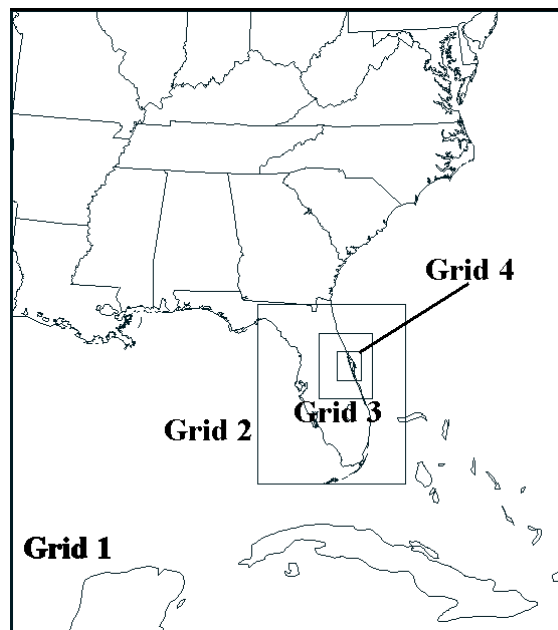
Figure 2. The RAMS domains for the 60-km mesh grid (grid 1), the 15-km mesh grid (grid 2), the 5-km mesh grid (grid 3), and the 1.25-km mesh grid (grid 4) covering the area immediately surrounding KSC/CCAFS.

2.4 Data Preparation for Sea-Breeze Verification

The original operational RAMS forecast output was saved only once per hour due to disk space limitations on the operational system. This relatively coarser time resolution presented a limiting factor for the robustness of an objective verification technique for verifying sea-breeze propagation. As a result, the daily 1200 UTC RAMS forecasts were re-run in order to generate NWP model output every five minutes, consistent with the time resolution of the observed tower data.

To conduct a head-to-head comparison between the observed and forecast fields, the gridded RAMS forecasts from the 1.25-km grid were interpolated to the location and height of the KSC/CCAFS tower observations. Then, the observed and point forecast winds were analyzed objectively onto the 1.25-km RAMS forecast grid using identical parameters of the Barnes (1964) algorithm. As a result, the objective analysis grid of observations and forecasts has coverage only within the domain of the KSC/CCAFS wind-tower network shown in Figure 1.

The motivation for re-analyzing point forecast data on the 1.25-km RAMS forecast grid was threefold:

- The original RAMS gridded forecasts contain wind information over both land and water, whereas the KSC/CCAFS tower observations are located solely over land. By interpolating RAMS forecasts from the original grid to the tower locations and then analyzing the observed and point forecast data back to the RAMS grid, the resulting objective analysis will represent a fair comparison between the observed and forecast wind fields.

- Re-analyzing point forecast data at each tower location results in observed and forecast wind fields with similar resolvable scales of motion.

- Objectively analyzing data onto a grid with evenly-spaced points provides a favorable platform for both analysis and display purposes.

3. TECHNIQUE TO VERIFY MODEL SEA BREEZES

A method that uses only wind directions, dubbed Contour Error Map (CEM), was developed in order to quantify the ability of RAMS to predict the sea-breeze (SB) phenomenon over the KSC/CCAFS domain. CEM employed a binary wind direction threshold to distinguish between easterly (onshore) and westerly (offshore) wind directions. This method incorporated both spatial and temporal wind data at each grid point of the objectively analyzed grids to identify observed and forecast SB transition times. A filtering technique was implemented to identify the correct transition times from offshore to onshore wind flow. To ensure focus on the SB boundary only, an erosion technique was introduced to remove extraneous boundaries not associated with the primary SB front, such as river breezes and precipitation outflow boundaries.

Since the coastline of east-central Florida is approximately oriented along a north-south direction,

wind directions between 0° and 180° were considered onshore winds, while 180° to 360° wind directions were defined as offshore. A histogram of the point-by-point differences in SB transition times between the forecast and observed fields was generated. A Gaussian histogram function $\hat{h}_k$ was fitted to the CEM histogram h_k in order to quantify and parameterize the comparison in terms of four parameters:

$\tau \equiv$ mean bias,

$\sigma \equiv$ standard deviation of bias,

$f_O \equiv$ fractional area of only OBS SB transition, and

$f_R \equiv$ fractional area of only RAMS SB transition.

The form of the Gaussian histogram function used in this study is given by:

$$\hat{h}_k = \frac{1 - f_O - f_R}{\sigma \sqrt{\pi}} \Delta t \; e^{-(t_k - \tau)^2 / \sigma^2} \qquad (1)$$

where t_k is the time corresponding to h_k, the subscript k corresponds to the kth 5-minute bin (the forecast – observed SB transition time difference), and Δt = 5 min (the time interval between successive observed and forecast wind fields).

For days with an overlapping observed and forecast SB transition within the grid domain, the Gaussian function fit was performed to produce a set of parameters that describe the quality of the RAMS forecast SB. Days with small mean biases and small standard deviations of the bias indicate more accurate forecasts of the SB transition timing and movement. In addition, the mean wind direction and wind speed were computed on the seaward side of the SB transitions in order to determine the skillfulness of RAMS in predicting the movement of the SB boundary and the representativeness of the post-SB wind environment.

To improve upon the fundamental 0−180° wind direction threshold, a time estimation filter was developed to determine the SB transition times in both the observed and forecast grids. Each grid point was processed individually by a detector composed of a parallel lowpass (LP) boxcar filter and a high-order bandpass (BP) filter (Hillman and Lane 1989) centered on a frequency of 1.0/day. The LP filter was used to remove microscale, convective features with a frequency on the order of 1.0/minute, whereas the BP filter was designed to simulate the land-sea breeze diurnal periodic cycle, as observed in nature. After each grid point was pre-processed by the SB filter, the spatial image was reconstructed.

The CEM algorithm consists of four segments:

(1) <u>Point Processing</u>: Calculates the sine of wind direction at each point in *x*, *y*, and *t* space.

(2) <u>Temporal Processing</u>: Processes a continuous time series at each *x-y* grid point to determine a best estimate of the offshore to onshore wind transition time.

(3) <u>Spatial Processing</u>: Computes two-dimensional spatial gradients of SB filtered and recombined spatial images.

(4) <u>Comparison and Analysis</u>: Verifies RAMS against the observed fields using the Gaussian fitted function and four comparison parameters described above, as well as computing the mean post-SB wind direction and speed.

3.1 SB Transition Time Estimation Filter

Both the LP and BP filters are implemented as zero-phase filters. The BP filter provides a SB transition time predictor, which is compared to the LP filtered wind direction signal at every spatial grid point. If the time difference between the predicted BP-SB time and the LP-SB time exceeds 6 hours, no SB for that day is assumed.

The SB time is taken as the LP time that most closely matches the BP time. The SBF algorithm fills in missing data by performing a linear interpolation between end points around the missing data before the LP and BP segments are performed. Figure 3 displays filter outputs for 10−13 May 2000. The raw data plotted in Figure 3 is the sine of the wind direction ϕ. In general, $\sin\phi$ would be replaced by $\sin(\phi - \phi_0)$, where ϕ_0 is the local orientation of the coastline. In our particular case, $\phi_0 = 0$.

The LP filter is implemented as a moving average filter and the BP filter is a zero-phase recursive filter with $Q = 2$, made up of dual eighth-order filters. The center frequency f_0 is set to match the 24-hour land-sea breeze diurnal cycle. The zero-phase filter is implemented by summing the outputs of two filters with identical characteristics, where one filter processes a block of data forward in time, and the other filter processes the data backward in time from the end of the block.

Every grid point in the observed and forecast data is processed using the SB time estimation filter. Recombining processed time-domain data into spatial images results in SB transition time plots, such as those presented in Section 4.2. Note that the primary effect of the SBF is to suppress the effects of outflow boundaries (convective rainfall).

3.2 Spatial Gradient of SB Transition Times

The inverse of the gradient of the SB transition time is proportional to the sea breeze boundary velocity, as shown in Figure 6:

$$\overline{\overline{v}}(x,y) = \frac{\nabla t_{SB}(x,y)}{\left|\nabla t_{SB}(x,y)\right|^2} \qquad (2)$$

where $t_{SB}(x,y)$ is the SB transition time. Even though Equation (2) describes a quantitative method of computing the SB boundary velocity, the gradient of $t_{SB}(x,y)$ is a more useful quantity. If the east to west direction is taken as positive, then a positive value of $\left[\nabla t_{SB}(x,y)\right]_x = \nabla_x t_{SB} = \frac{\partial t_{SB}}{\partial x}$ indicates a SB boundary

propagating from east to west. However, $\nabla_x t_{SB} < 0$ indicates a west to east propagation of the wind direction boundary. Since the SBF suppresses effects of outflow boundaries (convective rainfall), a negative $\nabla_x t_{SB}$ is most likely indicative of a river breeze pushing the SB boundary backward. Therefore, a negative gradient of the SB transition time $\nabla_x t_{SB}$ is a strong indicator of river-breeze contamination. This characteristic can be utilized to eliminate the river-breeze contaminated portions of the CEM difference images, and isolate the SB transition times only.

3.3 Image Erosion to Suppress Contamination by River Breezes

Image erosion is a common processing technique used to shrink an image object in some predictable way (Gonzalez and Woods 1992). Image erosion was used to suppress the river breeze part of the SB transition time images, using the gradient of the transition times to trigger the erosion process. The river breeze can often develop in advance of the actual SB transition, and move from west to east, opposite of the direction of the SB. By scanning east to west, if a negative gradient was detected (i.e. a boundary moving west to east, which cannot physically be a SB transition), then all SB times to the west of that point were re-coded as "no SB". This simple technique resulted in a reasonable suppression of river-breeze phenomenon which contaminated the primary SB boundary propagation.

Figure 4 shows an example of the observed SB transition times from 11 May 2000, before and after image erosion. Clearly, a river breeze developed to the west of KSC, resulting in an early easterly wind component over Mainland Florida and erroneously early SB transition times in the original image (Fig. 4a). The erosion technique removes from consideration the transition time data from the western boundary to the edge of the river-breeze contamination area (Fig. 4b). A detailed discussion on this sea- and river-breeze event is presented in the next section.

4. MULTI-DAY SEA / LAND BREEZE EVENT

This section presents an observational analysis of a multi-day sea- and land-breeze event from 10−13 May 2000, focusing on 10 and 11 May. In addition, the 1.25-km RAMS forecasts of sea breezes across east-central Florida is verified against the tower observations using the new technique described in Section 3.

4.1 Observational Perspective

A SB passage was evident on each day of the time period, with the most distinct SB front occurring on the afternoon of 10 May. Offshore flow prevailed from a west-southwesterly direction prior to the SB passage (Figs. 5a and b). By 1800 UTC, the SB front began affecting the extreme eastern tip of Cape Canaveral, FL (Fig. 5c) and progressed slightly inland during the next hour (Fig. 5d). During the same time period from 1600 UTC to 1900 UTC on the 11th, the large-scale offshore
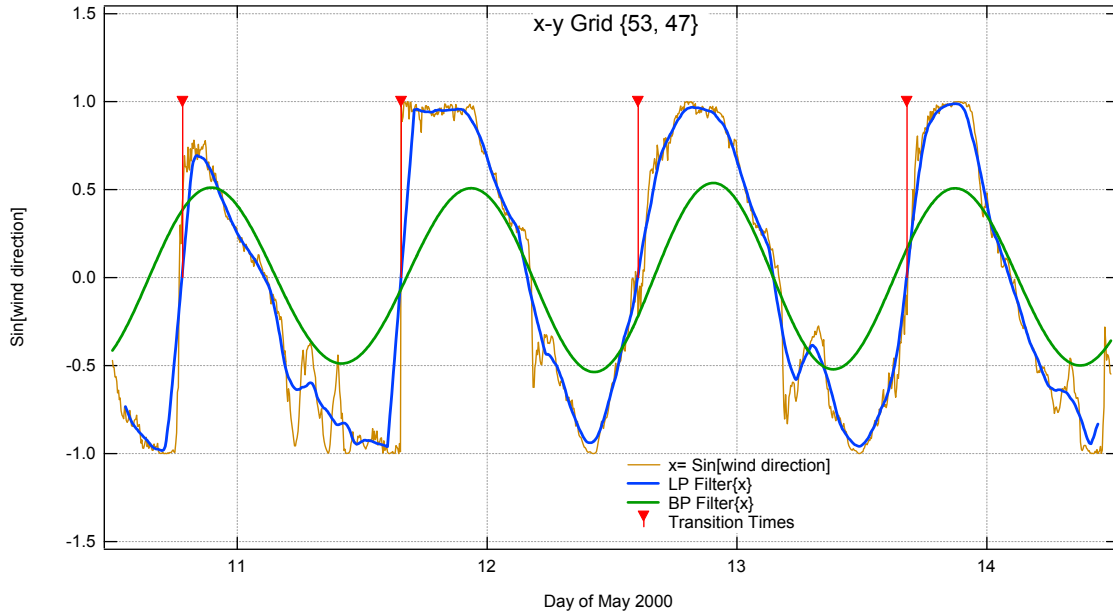
Figure 3. Results of the SB filter during 10−13 May 2000, as applied to wind direction data at x-y grid point (53,47). Red sticks indicate the best-guess SB transition times.
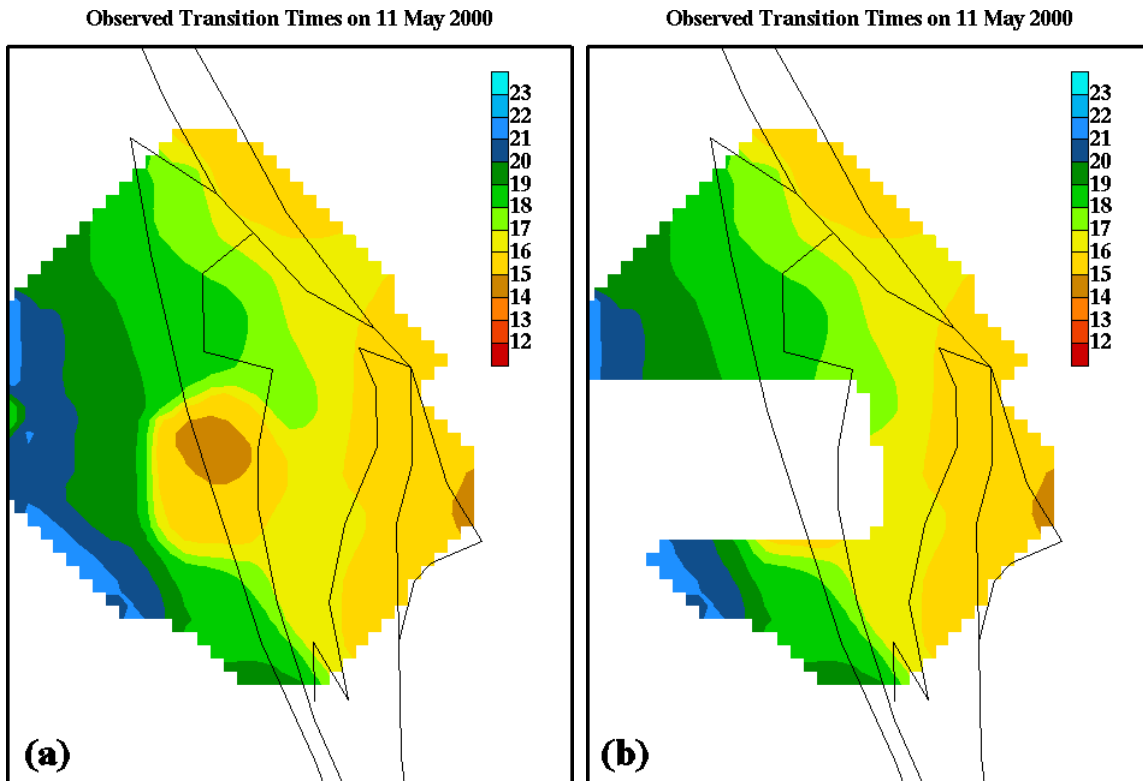
Figure 4. Observed SB transition times on 11 May 2000 (in UTC time) as determined by the CEM algorithm: (a) Transition times prior to image erosion, and (b) Transition times after image erosion.

flow was weaker, leading to an earlier onset of the SB (Fig. 6). In fact, the wind field on 11 May also included an Indian River-breeze circulation that promoted easterly flow over mainland Florida by 1600 UTC (Fig. 6a) and impeded the westward progress of the SB front over the north end of the Indian River and KSC (Figs. 6b and c). The onshore flow behind the SB front covered much of the KSC/CCAFS domain by 1900 UTC (Fig. 6d).

The low-level vertical structure of the SB frontal passage is clearly illustrated by time-height cross sections at the 150-m tall Tower #313, located in the north portion of KSC (Fig. 1). Figure 7 depicts a time-height cross section of winds from 1600 UTC to 2355 UTC on 10 May. The area of shading denotes the westerly u-winds preceding the SB front until about 1900 UTC.

(a) Observed Winds at 1600 UTC

(b) Observed Winds at 1700 UTC

(c) Observed Winds at 1800 UTC

(d) Observed Winds at 1900 UTC
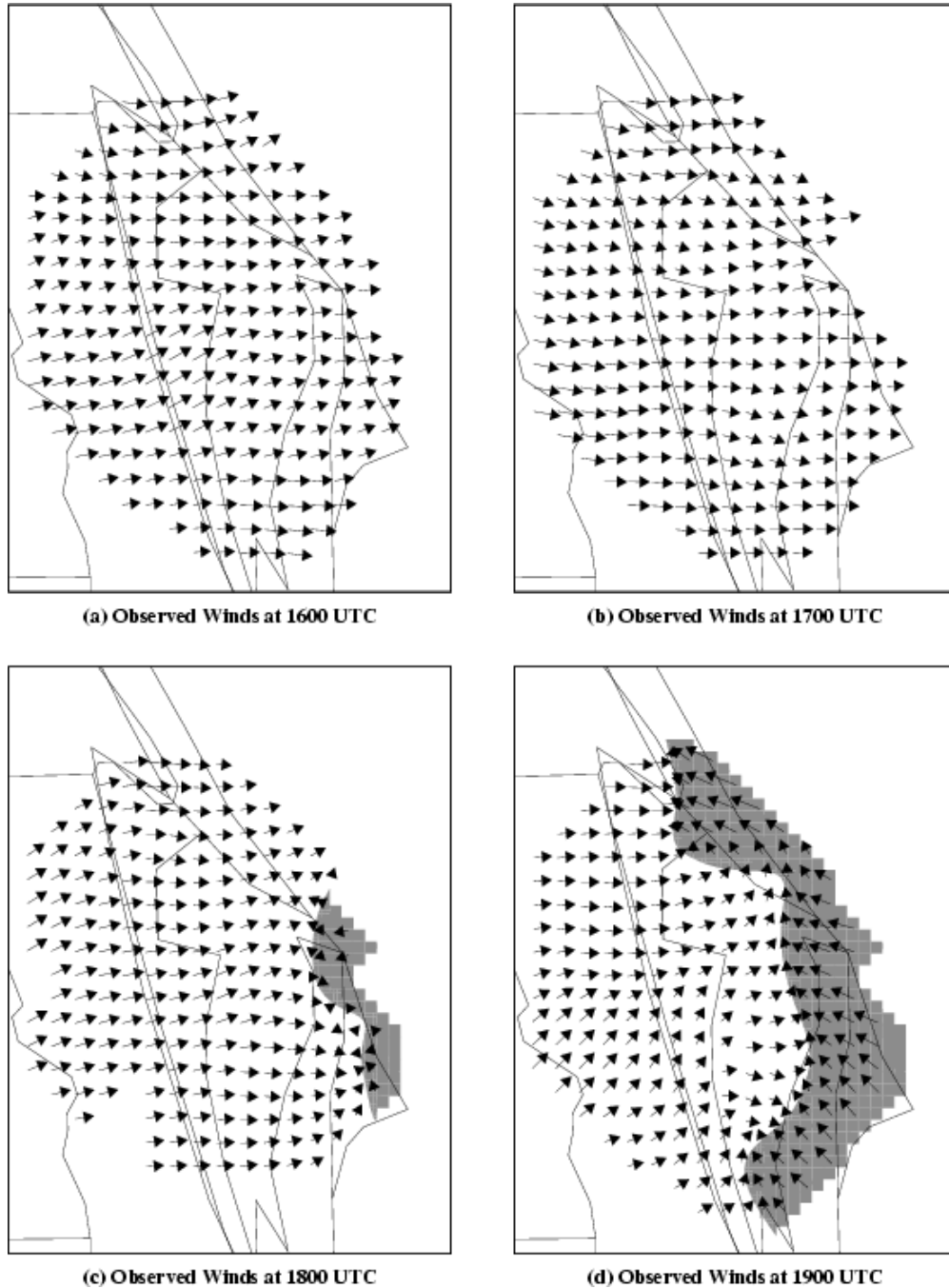
Figure 5. Grid analysis of observed KSC/CCAFS tower winds depicting sea-breeze passage on 10 May 2000.

Just after 1900 UTC, there is an abrupt temporal gradient in the u-wind component signifying the passage of the SB front. The southwesterly flow of about 5–10 kt prior to the SB is replaced with southeasterly flow of 10–20 kt after the SB frontal passage.

The low-level temperature and dew point also exhibited marked changes across the SB front. From the surface to 150 m, the temperature decreased by as much as 2°C in 15–30 minutes with the frontal passage

(Fig. 8). During the same transition period, the dew point increased even more substantially from about 16°C to over 20°C (Fig. 9), resulting in a large increase in the relative humidity (not shown).

Following the daytime SB of 10 May was a dual-surge land breeze (LB) between 0200 UTC and 1000 UTC 11 May. The initial LB passage occurred at about

(a) Observed Winds at 1600 UTC

(b) Observed Winds at 1700 UTC

(c) Observed Winds at 1800 UTC

(d) Observed Winds at 1900 UTC
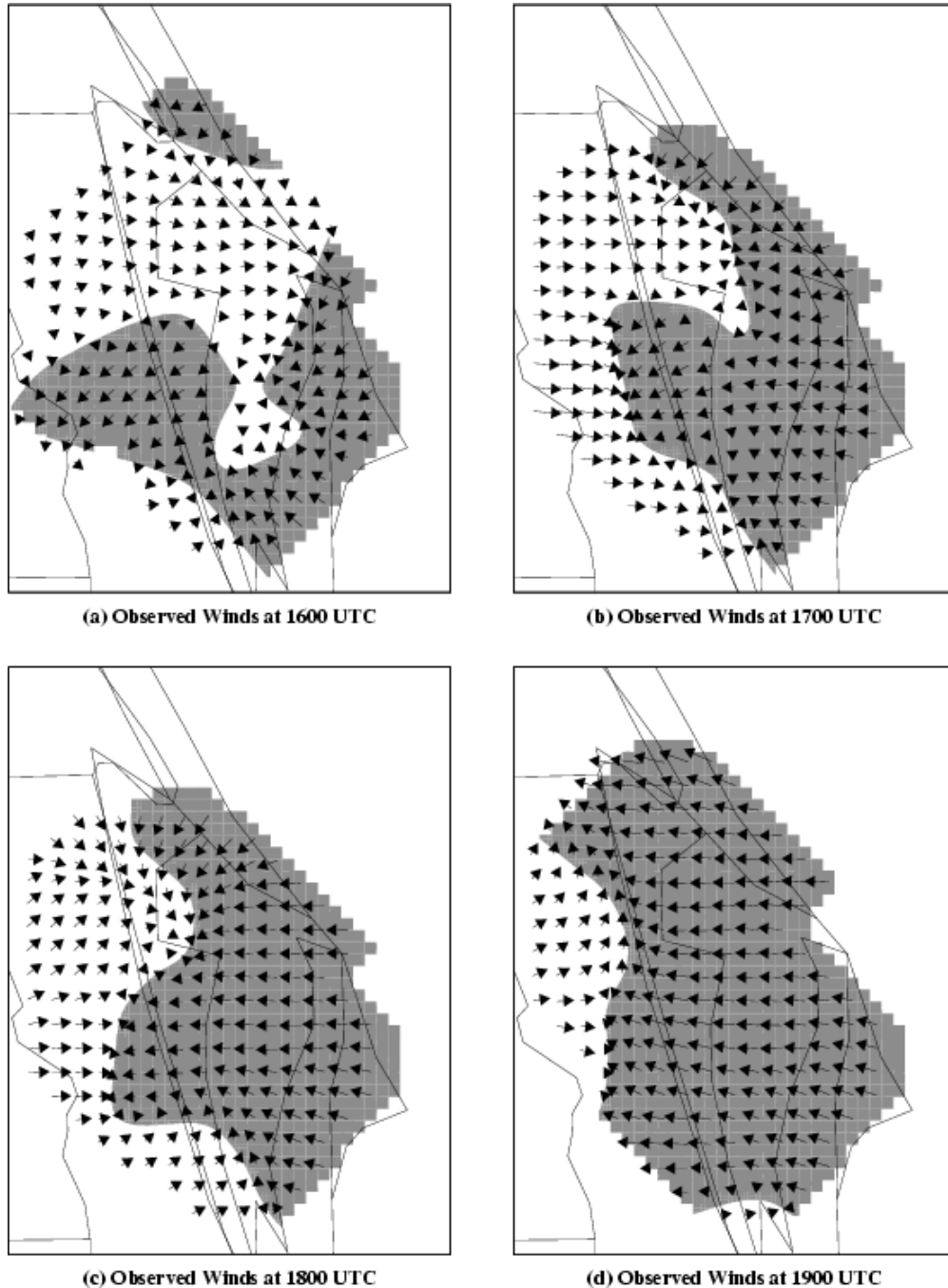
Figure 6. Grid analysis of observed KSC/CCAFS tower winds depicting sea-breeze passage on 11 May 2000.

0315 UTC 11 May, given by the fairly sharp transition from southerly shore-parallel flow to offshore flow in the time-height cross section at Tower #313 (beginning of shading in Fig. 10). Southwesterly flow prevailed for several hours after the leading land-breeze frontal passage until about 0800 UTC, when a secondary surge from the northwest overspread Tower #313. The wind speeds and the u-wind component increased after 0800 UTC, particularly above 50 m (Fig. 10).

Coincident with each land-breeze surge was a noticeable change in the low-level temperatures, particularly with the secondary surge associated with the wind-shift to a northwesterly direction. The temperature decreased by about 1°C at all levels with the first wind shift at 0315 UTC (Fig. 11); however, the temperatures decreased much more substantially after the second surge at 0800 UTC. In fact, the temperature

Figure 7. Time-height cross section of the u-wind component and wind barbs at tower 313 (location shown in Fig. 1) from 1600 UTC to 2355 UTC on 10 May 2000. Shading indicates positive (westerly) u-wind components in m s^{-1} given by the scale, whereas dashed contours represent negative (easterly) u-wind components.
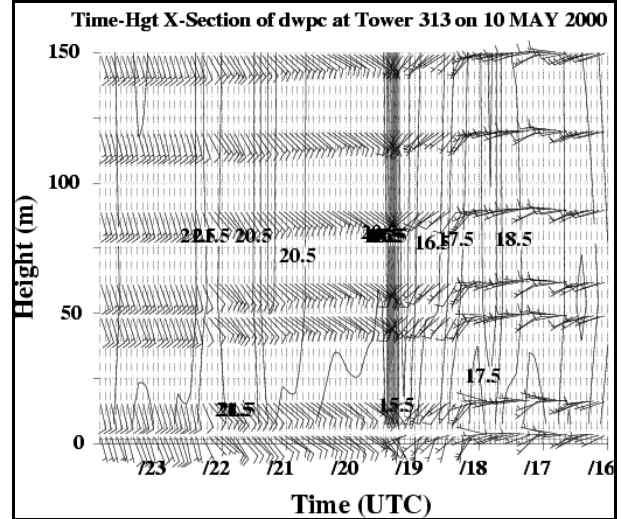
Figure 9. Time-height cross section of dew point (°C) and winds at tower 313 from 1600 UTC to 2355 UTC on 10 May 2000. Dew points are contoured every 0.5°C.

Figure 8. Time-height cross section of temperature (°C) and winds at tower 313 from 1600 UTC to 2355 UTC on 10 May 2000. Temperatures are contoured every 0.5°C.
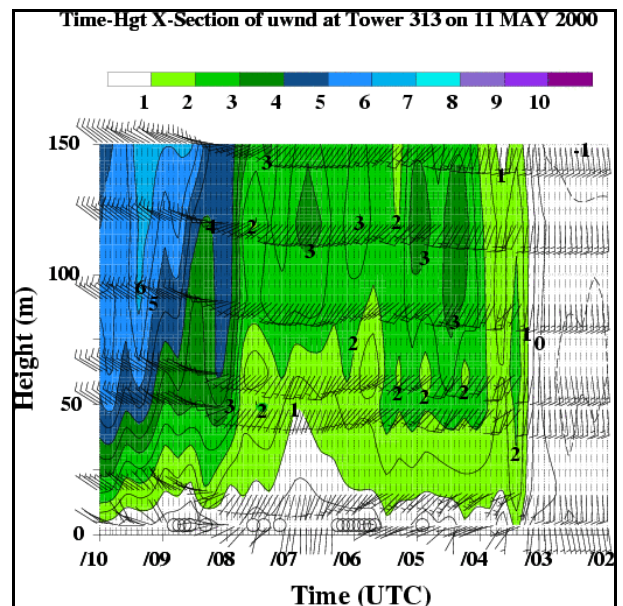
Figure 10. Time-height cross section of the u-wind component and wind barbs at tower 313 from 0200 UTC to 1000 UTC on 11 May 2000. Shading indicates positive (westerly) u-wind components in m s^{-1} given by the scale, whereas dashed contours represent negative (easterly) u-wind components.

structure after 0800 UTC in Figure 11 closely resembles that associated with the passage of a cold front or density current. Based on these results and a previous study on land breezes over east-central Florida (Case 2003), it appears that the initial LB surge was associated with the collapse of the SB circulation cell, whereas the secondary LB surge originated from radiational cooling over the interior of the Florida peninsula, resulting in the passage of a density current across east-central Florida late at night.

The observations from the 915-MHz profiler #3 over the south portion of KSC (Fig. 1) show some fascinating structure associated with the sea and land breezes of 10−11 May. Figures 12 and 13 show time-height cross sections of winds and the u- and v-wind components, respectively, at profiler #3 from 1500 UTC 10 May to 1200 UTC 11 May. In Figure 12, the time of passage and depth of the SB is clearly indicated by the sharp gradients between positive/westerly u-winds (shaded regions) and negative/easterly u-winds (dashed contours without shading). Southeasterly winds associated with the SB occur at levels up to ~600 m after 1800 UTC, and then abruptly shift back to an offshore direction shortly after 0300 UTC. The shift to northwesterly winds at 0800 UTC can be seen up to 500 m (Fig. 12).

By examining the time-height cross section of the v-wind component in Figure 13, a distinct feature stands out shortly after 0300 UTC, coincident with the time of the SB circulation collapse. Between 250 m and 750 m, a southerly low-level jet occurs for about 0.5 hours, with a magnitude of nearly 20 m s^{-1}. This low-level jet feature exhibited both spatial and temporal continuity among the five 915-MHz profilers (not shown, but is illustrated in the poster presentation). In addition, this feature occurred nightly from 11−13 May, but with decreasing intensity and at a slightly later time with each successive night.
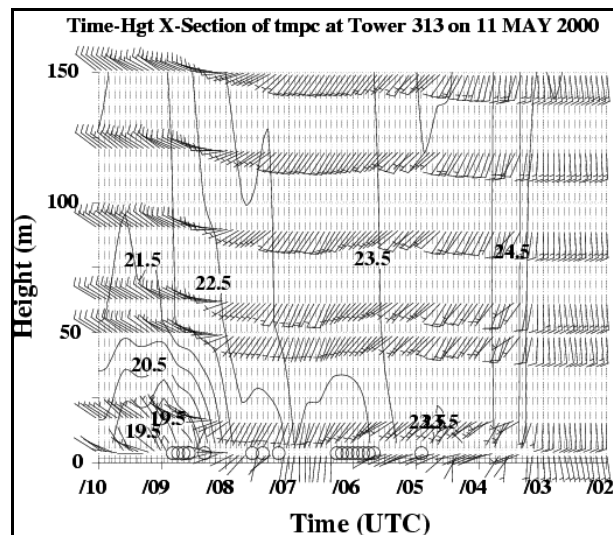
Figure 11. Time-height cross section of temperature (°C) and winds at tower 313 from 0200 UTC to 1000 UTC on 11 May 2000. Temperatures are contoured every 0.5°C.
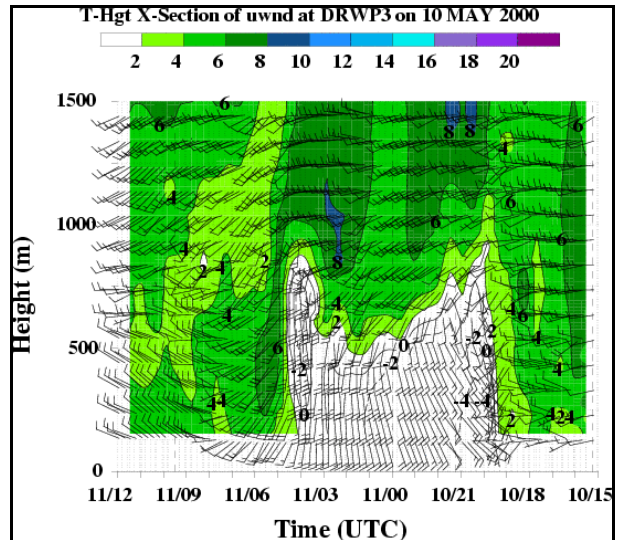
Figure 12. Time-height cross section of the u-wind component and wind barbs at 915-MHz DRWP #3 (location shown in Fig. 1) from 1500 UTC 10 May to 1200 UTC 11 May 2000. Shading indicates positive (westerly) u-wind components in m s^{-1} given by the scale, whereas dashed contours represent negative (easterly) u-wind components.
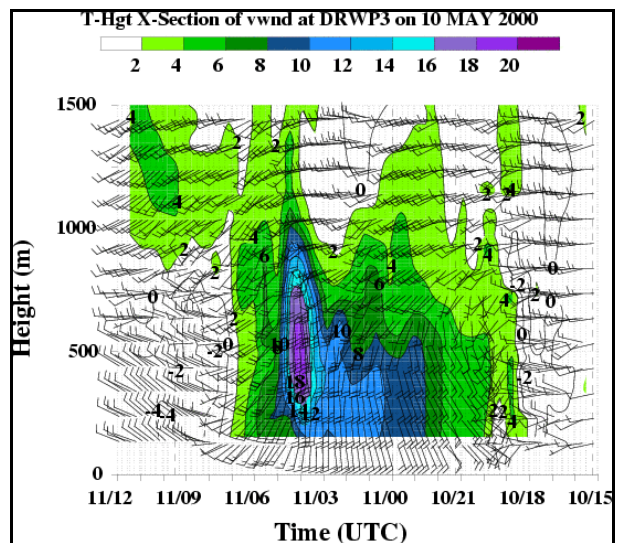
Figure 13. Time-height cross section of the v-wind component and wind barbs at 915-MHz DRWP #3 from 1500 UTC to 2300 UTC 10 May 2000. Shading indicates positive (westerly) u-wind components in m s^{-1} given by the scale, whereas dashed contours represent negative (easterly) u-wind components.

4.2 Verification of RAMS Forecast Sea Breezes

Figures 14 and 15 show the hourly RAMS forecast surface wind fields from 10 and 11 May, respectively, depicting the predicted SB transitions. By comparing the forecast wind field in Figure 14 with the observed winds in Figure 5, it is evident that RAMS was much too

early in the onset and inland propagation of the SB front on 10 May. By 1800 UTC, RAMS had already predicted the SB penetration throughout the entire KSC/CCAFS domain (Fig. 14c). Meanwhile, the observed SB had barely reached the coastal locations at the same time (Fig. 5c). Clearly, RAMS a substantial early bias in the SB movement on this day.

The 11 May RAMS predicted SB was much more skillfully forecast compared to 10 May. The RAMS hourly wind field in Figure 15 indicates that the SB transition moved inland in a very similar manner to the

observed SB (Fig. 6). The RAMS also predicted the SB transition quite well on 12 and 13 May (not shown).

Figure 16 shows the observed and forecast isopleths of the SB transition time for 10 and 11 May, as determined by the objective CEM method described in Section 3. As expected based on the wind-field comparison, the observed SB transition times (Fig. 16a) are several hours later than RAMS (Fig. 16b) across much of the analysis domain on 10 May.

(a) 1200 UTC RAMS Forecast at 1600 UTC

(b) 1200 UTC RAMS Forecast at 1700 UTC

(c) 1200 UTC RAMS Forecast at 1800 UTC

(d) 1200 UTC RAMS Forecast at 1900 UTC
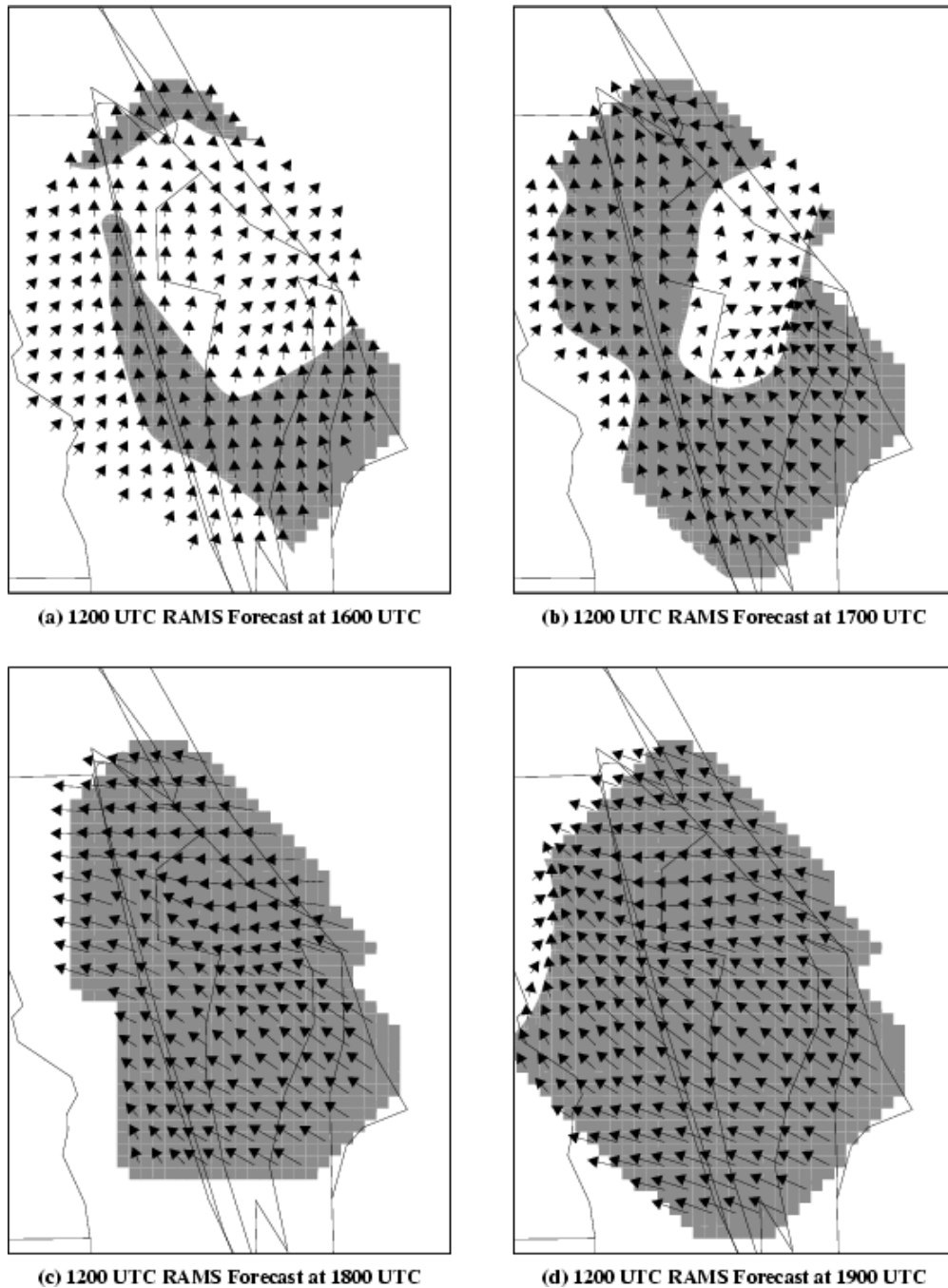
Figure 14. Grid analysis of RAMS winds depicting forecast sea-breeze passage on 10 May 2000.

Meanwhile, the SB transition times compare quite favorably on 11 May between the observed (Fig. 16c) and RAMS isopleths (Fig. 16d). Figure 17 depicts the spatial timing biases as derived from the CEM algorithm for both 10 May (Fig. 17a) and 11 May (Fig. 17b). Clearly, RAMS performed much better on 11 May in predicting the SB onset and movement. Most timing errors and less than 1.5 hours in magnitude on 11 May compared to timing errors of -2.0 to -4.5 hours on 10 May (negative errors indicate early time biases).

Table 1 provides a summary of the CEM Gaussian fit parameter statistics for the verification of the RAMS

SB transition times corresponding to each day from 10–13 May, based on Equation (2). The subjectively determined ranges of the observed and forecast SB transition times are also shown in the 6th and 7th columns, as a means of qualitatively validating the CEM results. Note that if neither a forecast nor observed SB had occurred on a particular day, zeros would appear for both f_O and f_R (no observed only or forecast only SB area). A complete forecast miss or false prediction of a SB on a particular day is represented by a value of unity for f_O (forecast failure) or f_R (false alarm prediction).
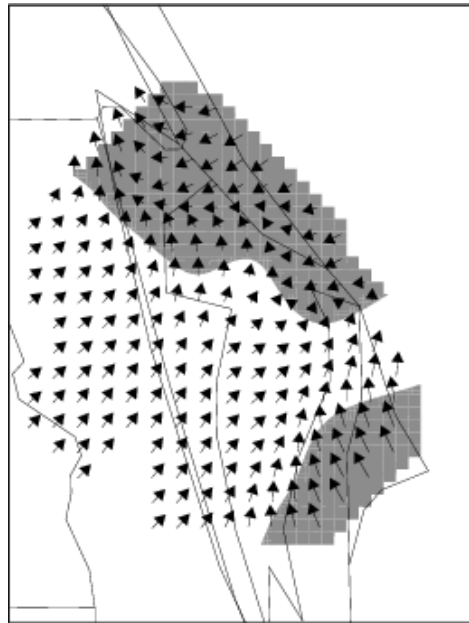
(a) 1200 UTC RAMS Forecast at 1600 UTC
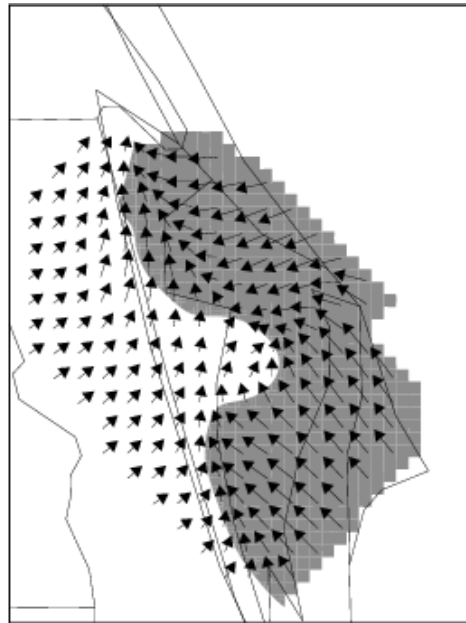
(b) 1200 UTC RAMS Forecast at 1700 UTC
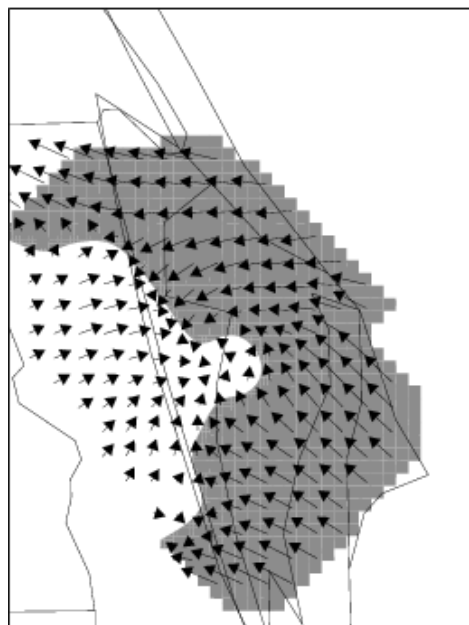
(c) 1200 UTC RAMS Forecast at 1800 UTC
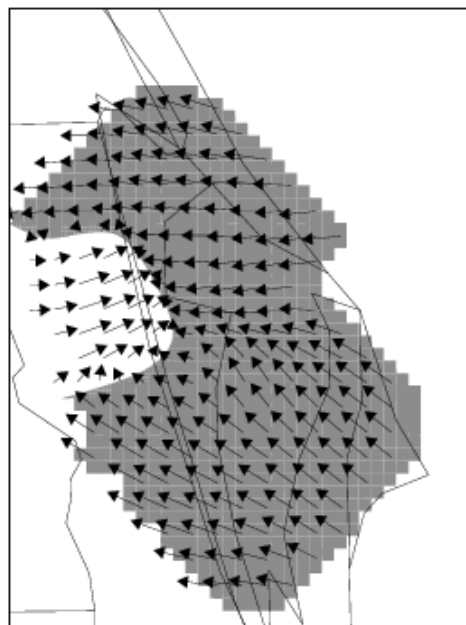
(d) 1200 UTC RAMS Forecast at 1900 UTC

Figure 15. Grid analysis of RAMS winds depicting forecast sea-breeze passage on 11 May 2000.

The RAMS forecasts from 11–13 May had the best skill in predicting the SB occurrence and timing, since those days had the smallest absolute values of the mean bias (τ) and the smallest standard deviation of the bias (σ). Note that the standard deviation of the bias indicates the amount of spatial variation in the timing errors across the KSC/CCAFS domain. Days that have a larger absolute value of τ indicate the greatest domain-wide timing biases in RAMS (e.g. the large negative timing bias from 10 May).

Using eroded SB transition times, the average of the observed and RAMS post-SB wind direction and speed for 10–13 May are shown in the final four columns of Table 1. Based on these results, it can be seen that RAMS predicted the post-SB wind direction better than the post-SB wind speeds. RAMS tended to have a substantially higher post-SB mean wind speed compared to observations, particularly on 10 and 11 May.
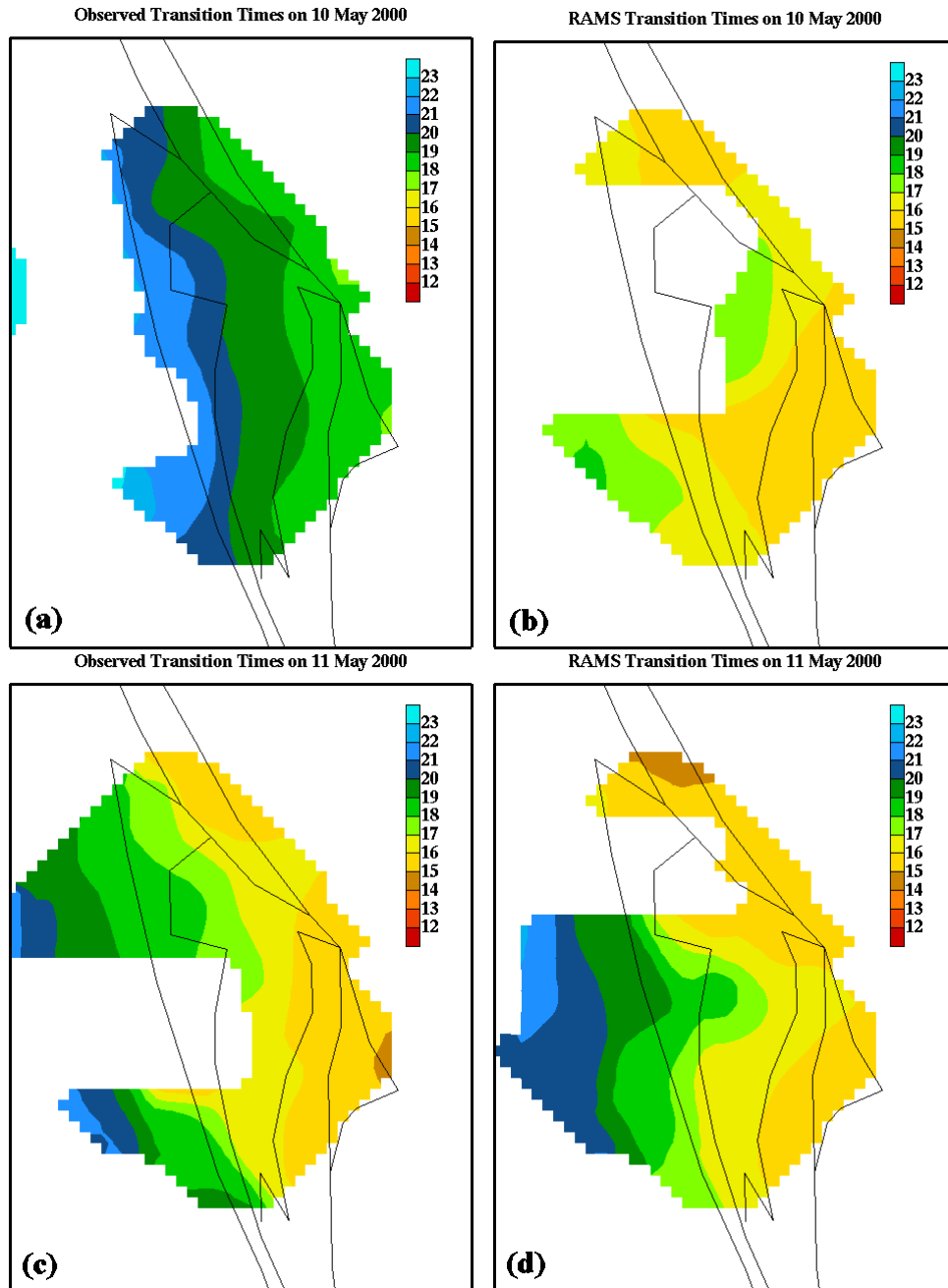
Figure 16. Observed and RAMS forecast isopleths of sea-breeze transition times (in UTC hours) for 10 and 11 May 2000, based on the results of the CEM verification algorithm. Transition times are shown for the (a) 10 May observed winds, (b) 10 May forecast winds, (c) 11 May observed winds, and (d) 11 May forecast winds.
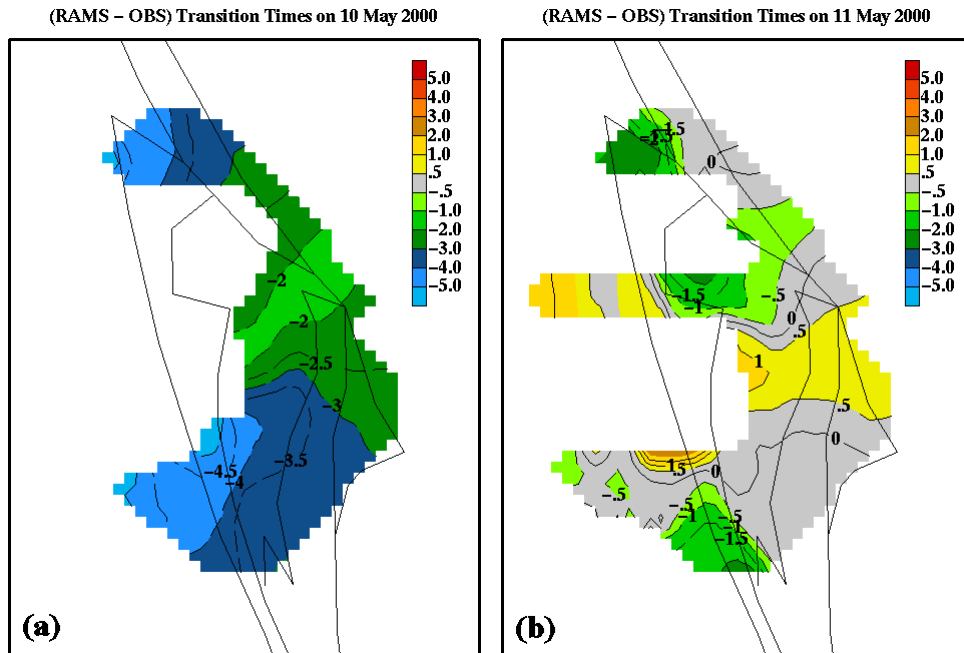
Figure 17. The differences between the observed and RAMS forecast sea-breeze transition times in hours for (a) 10 May, and (b) 11 May. Negative values indicate an early timing bias by RAMS.

TABLE 1. Gaussian fit parameters for eroded CEM histograms, subjectively-determined range of observed and RAMS times of the SB transition (in UTC), and the mean post-SB observed and forecast wind directions (WD, degrees) and wind speeds (WS, m s^{-1}) as calculated in CEM.

Day	τ (h)	σ (h)	f_O (%)	f_R (%)	Obs Times	RAMS Times	Post-SB Obs WD	Post-SB RAMS WD	Post-SB Obs WS	Post-SB RAMS WS
10	-3.1	1.4	31	8	1715 − 2230	1530 − 1815	142°	126°	4.5 m s^{-1}	6.2 m s^{-1}
11	-0.0	0.9	21	26	1445 − 1945	1515 − 1915	106°	126°	3.4 m s^{-1}	6.0 m s^{-1}
12	0.0	0.5	8	17	1400 − 1530	1415 − 1530	80°	97°	3.0 m s^{-1}	4.9 m s^{-1}
13	-0.6	0.5	2	12	1500 − 1730	1500 − 1630	85°	86°	3.3 m s^{-1}	4.2 m s^{-1}

5. SUMMARY

This paper presented a comprehensive analysis of a multi-day sea- and land-breeze event from 10−13 May 2000 across east-central Florida. Using the unique combination of observational data and analysis, forecast, and model-verification tools, the intricate details and structures of these phenomena were highlighted. Time-height cross sections of winds, temperatures, and dew points illustrated the sharp gradients that can occur with the SB and LB frontal passages. In addition, the 915-MHz profiler data depicted a substantial low-level jet that accompanied the collapse of the SB circulation during the evening hours of 10 May.

A new automated model verification method was developed to identify SB transition times in both observed and forecast grid wind fields. The results of this algorithm compared favorably to subjective analysis and successfully verified the RAMS forecast SB transition zones across the KSC/CCAFS domain. A phenomenological verification method such as CEM can save a substantial amount of time and manpower resources. The CEM also helps to improve the quality of verification results by focusing on the phenomenon rather than traditional error statistics, which cannot adequately quantify the utility of mesoscale model forecasts.

6. REFERENCES

Barnes, S. L., 1964: A technique for maximizing details in numerical weather map analysis. *J. Appl. Meteor.,* **3,** 396-409.

Benjamin, S. G., and Coauthors, 1998: The operational RUC-2. Preprints, *16th Conf. on Weather Analysis and Forecasting*, Phoenix, AZ, Amer. Meteor. Soc., 249-252.

Case, J. L., 2002: Final report on land-breeze forecasting. NASA Contractor Report CR-2002-211181, Kennedy Space Center, FL, 66 pp. [Available from ENSCO, Inc., 1980 N. Atlantic Ave., Suite 230, Cocoa Beach, FL 32931.]

Chen, S., and W. R. Cotton, 1988: The sensitivity of a simulated extratropical mesoscale convective system to longwave radiation and ice-phase microphysics. *J. Atmos. Sci.*, **45**, 3897-3910.

Cotton, W. R., M. A. Stephens, T. Nehrkorn, and G. J. Tripoli, 1982: The Colorado State University three-dimensional cloud/mesoscale model — 1982. Part II: An ice phase parameterization. *J. Rech. Atmos.*, **16**, 295-320. Gonzalez, R. C. and R. E. Woods, 1992: Digital Image Processing. Addison-Wesley Publishing Company, 716 pp.

Gonzalez, R. C. and R. E. Woods, 1992: Digital Image Processing. Addison-Wesley Publishing Company, 716 pp.

Heckman, S. T., M. W. Maier, W. P. Roeder, J. B. Lorens, and B. F. Boyd, 1996: The operational use of a boundary layer profiler network at the Eastern Range and Kennedy Space Center, *27th Conference on Radar Meteorology*, Vail, CO, 346-348.

Hillman, G. D. and J. E. Lane, 1989: Real-Time Determination of IIR Coefficients for Cascaded Butterworth Filters. *IEEE Intl. Conf. On Acoustics Speech and Signaling Processing*, Glasgow, Scotland, 1353-1356.

Lambert, W. C., F. J. Merceret, G. E. Taylor, and J. G. Ward, 2003: Performance of five 915-MHz wind profilers and an associated automated quality control algorithm in an operational environment. *Submitted to J. Atmos. Oceanic Tech*.

Lambert, W. C., 2002: Statistical short-range guidance for peak wind speed forecasts on Kennedy Space Center/Cape Canaveral Air Force Station: Phase I results. NASA Contractor Report CR-2002-, Kennedy Space Center, FL, 39 pp. [Available from ENSCO, Inc., 1980 N. Atlantic Ave., Suite 230, Cocoa Beach, FL 32931.]

Lambert, W. C., and G. E. Taylor, 1998: Data Quality Assessment Methods for the Eastern Range 915-MHz Wind Profiler Network. NASA Contractor Report CR-1998-207906, Kennedy Space Center, FL, 49 pp. [Available from ENSCO, Inc., 1980 N. Atlantic Ave., Suite 230, Cocoa Beach, FL, 32931].

Mellor, G. L., and T. Yamada, 1982: Development of a turbulence closure model for geophysical fluid problems. *Rev. Geophys. Space Phys.*, **20**, 851-875.

Pielke, R. A., and Coauthors, 1992: A comprehensive meteorological modeling system — RAMS. *Meteor. Atmos. Phys.*, **49**, 69-91.

Radian International, 2001: *LAP*®-*3000 Operation and Maintenance Manual*, 5600 Airport Boulevard, Boulder, CO 80301, Document Control No. 80018201 Revision F, 376 pp.

Tremback, C. J., 1990: Numerical simulation of a mesoscale convective complex: Model development and numerical results. Ph.D. dissertation, Atmos. Sci. Paper No. 465, Department of Atmospheric Science, Colorado State University, Fort Collins, CO 80523, 247 pp.

_____, and R. Kessler, 1985: A surface temperature and moisture parameterization for use in mesoscale numerical models. Preprints, *Seventh Conf. on Numerical Weather Prediction*, Montreal, Quebec, Amer. Meteor. Soc., 355-358.

Zhong, S., and E. S. Takle, 1992: An observational study of sea- and land-breeze circulation in an area of complex coastal heating. *J. Appl. Meteor.*, **31,** 1426-1438.

_____, and _____, 1993: The effects of large-scale winds on the sea-land-breeze circulations in an area of complex coastal heating. *J. Appl. Meteor.*, **32,** 1181-1195.